J. Fluid Mech. (1986), *vol.* 172, *pp.* 63–92
Printed in Great Britain

Calculation of flow and pollutant dispersion in meandering channels

By A. O. DEMUREN† AND W. RODI
Institute for Hydromechanics, University of Karlsruhe, Karlsruhe, F.R. Germany

(Received 19 August 1985 and in revised form 7 May 1986)

Experiments on and calculation methods for flow and pollutant spreading in meandering channels are reviewed. The shortcomings of existing calculation methods are discussed in the light of the complex three-dimensional nature of the flow situation. A mathematical model is presented which takes full account of the three-dimensionality of the flow and pollutant concentration fields. This model is based on the solution of the momentum equations governing the flow in the lateral, vertical and longitudinal directions with a three-dimensional numerical procedure together with the continuity equation. The turbulent stresses appearing in the momentum equations are calculated with a version of the k–ϵ turbulence model that accounts for streamline curvature effects on turbulence. The pollutant concentration field is subsequently obtained from a solution to its transport equation. The model is tested by application to three different meander situations for which velocity and concentration measurements are available from the literature, with channel width-to-depth ratios in the range 4–20, smooth and rough beds and various pollutant-discharge locations. Detailed comparisons of the velocity and concentration fields show generally good agreement. The effect of streamline curvature on the turbulent mass fluxes was found to be important only in the narrow channel with a smooth bed. Bed-generated turbulence appears to overrule this in the other two cases of a wide channel with a smooth bed and a narrow channel with a rough bed. The flow patterns show the presence of a single large eddy at most cross-sections in these cases, whereas the predictions indicate the presence of usually more than one eddy in the former case.

1. Introduction

1.1. *Background*

The meandering of rivers is one of the most interesting natural phenomena whose analysis poses a great challenge to engineers and scientists. The increased importance of rivers in man's daily activity for navigation, water supply, fish production, waste disposal, energy production etc. has made it necessary to optimize the use of these water bodies through control and man-made modifications. This underlines the need for understanding the various mechanisms governing the flow in rivers, the dispersion of pollutants, sediment transport etc. and to be able to predict these processes. Although many theoretical and experimental investigations have been carried out over the years on river meandering, some aspects of this phenomenon are still not quite understood and are difficult to analyse mathematically. Often, simplifying assumptions are introduced that have been found inappropriate. One major drawback appears to be the assumption of two-dimensional flow in most of the analytical

† Present address: Engineering Analysis Unit, University of Lagos, Lagos, Nigeria

attempts. However, the mechanisms involved cannot be explained adequately without considering the secondary motion which is an essential feature of the flow in meandering channels. This motion, in turn, cannot be directly encountered for in a two-dimensional analysis. The present paper reports on a three-dimensional mathematical model which does not suffer from this shortcoming. The work reported here must be considered as a first step towards the development of an accurate mathematical model which would not only allow the prediction of, but also enhance considerably the understanding of the complex phenomena in river meanders, especially the relationship between longitudinal and secondary motion, bed shear-stress distribution and sediment transport.

1.2. *Previous work*

1.2.1. *Theoretical studies*

Boussinesq (1868) presented a mathematical analysis of laminar flow in a mildly curved channel that explained the development of secondary motion in the bend. Thomson (1876) introduced a theory on how the secondary flow observed in channel bends leads to the meandering of rivers. He considered the flow around the bend to be irrotational (at least as far as the radial velocity distribution is concerned) and the pressure along any vertical line to be hydrostatic so that the water surface must slope down from the outer to the inner bank in order that the resulting pressure gradient balances the centrifugal force. He then assumed this pressure gradient to be independent of the depth and deduced that, because the velocity decreases with depth owing to bed friction, the fluid elements near the bed must take paths with smaller radia of curvature than those near the surface. This means that these elements move towards the inner bank while the elements near the free surface move towards the outer bank. The motion thus induced in cross-sectional planes requires, of course, vertical currents near the banks, upward near the inner bank and downward near the outer bank, which together result in a spiralling motion. Owing to the various simplifying assumptions involved, the strength of the spiralling motion predicted by the basically inviscid flow analysis did not correspond closely to the experimental observations. In fact, the analysis is somewhat inconsistent in that the flow is considered to be virtually inviscid but a friction has to be called upon to introduce a lower velocity near the bed.

Einstein & Harder (1954) observed in their experiments that the reciprocal of the curvature parameter $(\partial U/\partial r/U/r)$, which should have a value of -1 in free vortex flow and $+1$ in forced vortex flow with constant angular velocity, has values greater than 4 in shallow curved bends even in regions where apparently equilibrium conditions prevailed. This anomaly was explained by the presence of a boundary layer developing along the channel bed owing to the secondary flow, whose effects are confined to the region near the bed, with the main vortex near the water surface remaining unaffected. Einstein & Harder then postulated a theory whereby the tangential surface slope is greater than the frictional slope, and a balance of forces acting on the fluid elements showed how this could lead to the low values observed for the curvature parameter in their experiment. When further assumptions are introduced on the friction factor, this analysis can be used to compute the radial distribution of the longitudinal velocity in the central region of the channel away from the banks and also from the entrance to the bend. Their major contribution is the realization of the importance of the main flow distribution in determining the secondary motion and, in turn, the effect of the secondary flow on the former.

Ananyan (1957) and Rozovskii (1957) introduced perturbation techniques to analyse the flow in curved bends. As a first approximation, they assumed that the main flow was unaffected by the secondary motion. The solution obtained this way was subsequently modified by introducing a perturbation accounting for the effects of the secondary motion, using the depth-to-curvature-ratio (h/R_c) as the perturbation parameter. Many varieties of this perturbation method have subsequently been developed and applied (Yen 1965; Callander 1969; De Vriend 1973, 1981*a*; Engelund 1974; Ikeda 1975, amongst others) to analyse the flow in curved channels. In fact, this type of analysis appears to be by far the most popular cited in the literature. However, the underlying assumption, namely that the secondary motion acts only to perturb essentially fully developed straight channel flow, limits severely the applicability of this type of method. By its concept, the method is suitable only for mildly curved ducts and then again only after long exposure to curvature, that is not to the developing region. Hence, such methods cannot predict reliably the flow in strongly curved channels or in situations consisting of a series of meanders where history effects of preceding bends are transmitted downstream. A further deficiency of these methods is the assumption that the flow is either laminar or that turbulence effects can be accounted for by constant eddy viscosity or a simple eddy viscosity distribution derived from a power law for the vertical velocity distribution and a value of the friction coefficient.

De Vriend (1981*a*) found in analysing the Navier–Stokes equations for fully developed laminar flow in curved rectangular ducts that the deformation of the main velocity distribution by the secondary flow increases with the Dean number ($= Re\,(h/R_c)^{\frac{1}{2}}$). He thus concluded that perturbation methods are only applicable to flows with low Dean numbers (less than about 10). He then proposed a similarity analysis for flows with intermediate Dean numbers (up to 50). In this method, he neglected terms representing transverse inertia of the secondary motions, and by assuming similarity profiles for the main and the secondary flow he could simplify the Navier–Stokes equations to such a form that they could be solved easily with a numerical technique (integral-method approach). With the help of additional assumptions he then extended the method to make it applicable to developing laminar and turbulent flows. For turbulent flows, the effective Reynolds and Dean numbers are based on an estimated average eddy viscosity, and not on the molecular viscosity. He prescribed the eddy viscosity distribution as parabolic in the vertical direction and proportional to the local friction velocity. Subsequently, De Vriend (1981*b*, *c*) showed that the model predictions compared favourably with laboratory measurements in shallow ($B/h \approx 10$) and mildly curved channels; however he observed significant deviations from the measurements in less-shallow or strongly curved channels. In view of the many simplifying assumptions (including the rather simple turbulence model involved), these deviations are not surprising.

Leschziner & Rodi (1979) developed a three-dimensional numerical model for predicting the flow in strongly curved open channels. They solved the time-averaged Navier–Stokes equations with a numerical procedure similar to that proposed by Pratap & Spalding (1976) and applied by these authors to flow in strongly curved closed conduits. The procedure is essentially an extension of the once-through marching parabolic procedure of Patankar & Spalding (1972). However, in strongly curved ducts it is important to allow pressure effects to be transmitted upstream, and therefore in such situations the marching integration process must be repeated several times until a converged pressure field is achieved. Flow reversal in the main flow direction cannot be accommodated by this procedure. This restriction was

introduced only to economize on the necessary computer storage: all variables except the pressure need to be stored in two-dimensional arrays rather than in three-dimensional ones as would be required in a fully elliptic procedure which would also allow flow separation. For the same reason, diffusion in the longitudinal direction was neglected, which is in line with the boundary-layer approximations. Leschziner & Rodi's (1979) method employs the more refined k–ϵ turbulence model, which determines the turbulent velocityscale and lengthscale from differential transport equations. With their three-dimensional model, Leschziner & Rodi calculated the flow in a strongly curved rectangular channel consisting of a 180° bend between two straight sections. They obtained distributions of the main and secondary velocities that were in good agreement with the measurements of Rozovskii (1957). As will be shown below, the mathematical model to be presented in this paper is an extension of Leschziner & Rodi's model.

The secondary motion in meandering rivers has a very strong influence on heat and mass transfer and hence on the distribution of pollutants, as was first discussed in some detail by Fischer (1969). Viewed globally, this influence increases the mixing, but the actual process is not that of turbulent mixing but of convective transport of heat or mass by the secondary motion. The analysis of this transport requires three-dimensional consideration, but again the analyses carried out so far have been two-dimensional depth-averaged for the lateral mixing and one-dimensional cross-sectional averaged for the longitudinal dispersion of pollutants under situations of unsteady pollutant spreading. The depth and cross-sectional averaging of the original three-dimensional convection–diffusion equation for pollutants (temperature or concentration) introduces so-called dispersion terms in the simplified equations, and these are approximated by relating them to gradients of the transported quantity, thereby introducing dispersion coefficients. These coefficients then basically act to enhance the turbulence exchange coefficients already present in the equations. Fischer (1969) used Rozovskii's (1957) measured secondary velocity profiles and the shear-flow analysis of Taylor (1954) and Elder (1959) to determine the influence of curved channel flow on the dispersion coefficient. He found that the dimensionless lateral dispersion coefficient $\Gamma/\bar{U}_* h$ should be proportional to $(\bar{U}/U_*)^2 (h/R_c)^2$ where $\bar{U}$ is the mean velocity in the channel, U_* is the friction velocity, h is the channel depth and R_c is the radius of curvature. Yotsukura & Sayre (1976) later found that various laboratory measurements rather suggested that $\Gamma/U_* h$ should be proportional to $(\bar{U}/U_*)^2 (B/R_c)^2$, where B is the width of the channel. A compilation of the data and a discussion on this relation can also be found in the book by Fischer *et al.* (1979). The measurements indicate that the dimensionless dispersion coefficient can increase from the value of 0.15 usually observed in straight channels to values of more than 2 in laboratory flumes; in real rivers considerably higher values have been observed. A similar influence on the longitudinal dispersion coefficient was determined from experiments as discussed in Fischer *et al.* (1979). Smith (1981) employed a ray-path method to show that pollutant concentration due to a steady source discharging near the centre of a curved channel would be greatest near the outer bank. Smith (1982, 1983) investigated lateral and longitudinal dispersion in meandering channels, including history effects and the effects of variations in depth and width. To a large extent these works complement analytically the empirical deductions and computations of Fischer (1969). All of Smith's analyses are based on a depth-averaged treatment and require lateral dispersion coefficients as input. The dispersion relations proposed so far are all fairly crude; they do not account sufficiently for differences in the flow development and do not allow an adequate description of the actual transport processes. This is possible only with a three-dimensional model.

1.2.2. *Experimental studies*

A large number of experimental investigations on river-meander problems have been reported in the literature: A general review of these can be found in Callander (1978). Here are reviewed briefly those studies that give particular insight into the development of the secondary motion and its influence on the main flow distribution as well as on the dispersion of pollutants.

Measurements of the development of the longitudinal velocity in curved channels (e.g. Rozovskii 1957; Ippen *et al.* 1962; Chang 1971; Fukuoka 1971; Siebert & Götz 1975; Meckel 1978; De Vriend 1979; Siebert 1980) have shown that the velocity maximum usually occurred near the inner bank at the inlet to the bend and near the outer bank at the outlet. This is due to the increase of the water elevation at the outer bank and the decrease at the inner bank by centrifugal forces in curved channels. Associated with the building-up and the subsequent decay of a transverse surface slope in the bend is the presence of an adverse pressure gradient and an associated fluid deceleration at the outer bank and a favourable pressure gradient and fluid acceleration at the inner bank. Near the outlet, beyond the location of maximum transverse surface slope, these mechanisms are reversed so that the velocity maximum tends to shift to the outer bank. The spiral secondary motion transports high-momentum fluid from the upper layers to the outer bank and low-momentum fluid from the near-bottom layers towards the inner bank and therefore supports this reversal, i.e. it helps to shift the velocity maximum to the outer bank. However, only in very gentle bends, where approximately fully developed conditions with negligible longitudinal pressure gradients can develop, does the spiral motion dominate the longitudinal velocity distribution so that under these conditions the maximum would be near the outer bank. In general, the streamwise development or decay of the surface slope are important throughout the bend and are felt for considerable distances even upstream and downstream of the bend. Siebert (1980) has found that this influence persists much longer than the influence of the secondary motion. In meandering channels with one bend following another there is therefore considerable interaction between the individual bends. When the channel is very strongly curved, the adverse pressure gradient at the outer bank near the inlet and at the inner bank near the outlet of the bend can be so strong that the flow separates. This tendency to separation near the location of maximum superelevation was observed by Mockmore (1953), Shurky (1949), Ippen *et al.* (1962) and Yen (1970). The tendency decreased as the radius-to-width-ratio R_c/B increased and in subsequent bends of a meandering channel. It should be noted however that the experiments of Rozovskii (1957) in a strongly curved channel with $R_c/B = 1$ and $B/h = 13.3$ did not show any evidence of separation.

Secondary velocities in meandering channels were measured by Chang (1971), Fukuoka (1971), Siebert & Götz (1975), Mosonyi, Meckel & Meder (1975), Meckel (1978), Siebert (1980), Tamai *et al.* (1983) among others. The strength of the spiral motion (expressed as the ratio of the average kinetic energies of the secondary and main flow) was found by Mosonyi & Götz (1973) and by Mosonyi *et al.* (1975) to depend on the width-to-depth ratio B/h. Values as high as 2% were observed in the first bend of a meandering channel consisting of a series of 180° sections connected by straight tangents for $B/h = 4.6$ and less than 0.5% for $B/h = 20$. In both cases, R_c/B was 4, and measurements of the strength of the spiral showed that it decreased in subsequent bends; this reduction was much stronger in the deeper channel. The reason for this is that the sense of a spiral motion is reversed in subsequent bends so that the residual motion from the previous bend counteracts the setting-up of the

spiral in the next bend. From this it must also be expected that the strength of the spiral motion in meandering channels is less than that in channels containing only a single bend. Direct comparisons are difficult; hence here only an idea about the magnitudes of secondary velocities can be given. Rozovskii (1957) observed transverse velocities in his strongly curved 180° bend ($R_c/B = 1$) of 40–50% of the mean longitudinal velocity. Chang (1971), in a meandering channel with milder curvature, ($R_c/B = 3.7$ and $B/h = 20$) found that the magnitude of the transverse velocity may be as high as 15% of the mean longitudinal velocity at some locations. Meckel & Chun (1975) found that the influence of the spiral motion in a bend on those in subsequent bends is considerably less in channels with movable beds.

The spiral motion may be used to explain the depression of the maximum longitudinal velocity below the water surface observed in various experiments (e.g. Siebert & Götz 1975; Meckel 1978; Tamai *et al.* 1983). According to Meckel (1978), this depression leads to a local increase in the bed shear stress causing scour and erosion of the bed near this location. This contradicts previous theories according to which the secondary flow is directly responsible for bed scour and erosion.

In a number of experiments, a second, smaller counter-rotating eddy was observed near the surface at the outer bank (e.g. Chang 1971; De Vriend 1979; Siebert 1980). Mosonyi & Götz (1973) found that the existence of this eddy depends on the width-to-depth ratio B/h. While the eddy was present over much of the bend at low values of B/h, they found it to be completely absent at $B/h = 20$. Measurements of Tamai *et al.* (1983) confirmed these findings. De Vriend (1981*a*) has suggested that the development of the counter-rotating eddy may be due to a hydrodynamic instability. He argued that this may be similar in origin to the Görtler vortices present in boundary layers along concave walls, and that its onset signifies the beginning of the high-Dean-number flow range.

Few experiments have studied pollutant spreading in meandering channels. Fischer (1969) determined the influence of curvature on the dispersion coefficient in a flume with constant curvature. Chang (1971) took concentration measurements in a channel consisting of two 90° bends in alternating directions connected by short tangents, while Fukuoka (1971) and Fukuoka & Sayre (1973) reported concentration measurements in a sinuous channel consisting of a large number of meanders. In their flume, periodic flow existed in the latter stages where the dye was introduced. In all experiments, rapid mixing occurred in the vertical direction, but due to the skewing action of the secondary motion, the vertical dye distribution was non-uniform for considerable distances from the dye injection. As mentioned above, the secondary motion also causes a considerable lateral spreading of the dye so that the effective mixing is much stronger than in a straight channel. The dispersion coefficient quantifying this mixing, whose determination was one of the prime objectives of the above experiments, is generally much larger than the turbulent diffusion coefficient. It was found to reach a maximum value at about the middle of each bend and a minimum value at about the middle of the tangents between the bends. Field measurements in meandering rivers have been reported by Yotsukura, Fischer & Sayre (1970) and by Holley & Abraham (1973). The latter found that pollutants discharged on the inner bank experienced considerably less dispersion than those discharged on the outer bank.

1.3. *Present contribution*

The complex three-dimensional nature of the flow and pollutant concentration fields in meandering channels and especially the important influence of the secondary motion on the primary velocity field, the wall-shear-stress distribution and the pollutant dispersion has been highlighted by reference to previous studies. A review of theoretical studies has shown that most existing methods for calculating the flow in meandering channels are based on fairly restrictive assumptions so that they are not suitable for situations with strong curvature and development regions, where the full three-dimensional nature of the flow has to be accounted for. Also, the existing models for pollutant spreading in meandering channels allow only a global empirical description of the influence of the curvature via dispersion coefficients and do not describe the actual transport of pollutants by the secondary motion.

The present study presents a mathematical model that is not subject to the restrictions mentioned above as it takes full account of the three-dimensional nature of the flow and concentration fields. The model is an extension of the method of Leschziner & Rodi (1979) that solves numerically the three-dimensional Navier–Stokes equations together with a suitable turbulence model. This method has been developed for and applied to a single bend, and one of the extensions was to make it applicable to meandering channels with a sequence of bends with reversal of the curvature. There is no restriction to the number of bends as the concept of periodicity is employed when the number of bends is so large that the flow pattern repeats itself. In order to determine the pollutant concentration field in meandering channels, the three-dimensional convection–diffusion equation governing this field is also solved here. Further, the numerical procedure was improved by replacing the first-order-accurate upwind differencing scheme employed in Leschziner & Rodi's (1979) method by the higher-order-accurate quadratic upstream weighted differencing scheme (QUICK) proposed by Leonard (1979). This improved scheme for approximating the convection terms in the various governing equations reduces considerably the numerical diffusion generated by the method. Previous calculations by Demuren (1983) have shown that the use of this higher-order scheme enabled considerably better predictions of pollutant concentration distributions while the velocity predictions were only slightly affected.

The present study is restricted to the calculation of steady flow in channels with rectangular cross-section and fixed bed. Also, only situations are considered where the discharged pollutants are neutrally buoyant and conservative. The study is an important step towards the development of a powerful calculation method for the complex real-life flow, pollutant-spreading and sediment-transport processes in meandering rivers. For the idealized situation mentioned above, the model is tested extensively by simulating the meandering laboratory-flume situations studied experimentally by Chang (1971) and Fukuoka (1971). Predictions of the development of the primary and secondary velocity fields are compared with the laboratory measurements for various conditions. The calculated pollutant-concentration fields are also compared with the available measurements. Finally, the predicted bed shear-stress distribution in meandering channels is examined.

2. Mathematical model

2.1. *Mean-flow equations*

The time-averaged equations governing the steady, uniform-density, three-dimensional, turbulent flow and pollutant transport in the curved sections of a meandering channel may be written in cylindrical polar coordinates (r, y, θ) as follows:

continuity equation

$$\frac{1}{r}\frac{\partial r U_r}{\partial r}+\frac{\partial U_y}{\partial y}+\frac{1}{r}\frac{\partial U_\theta}{\partial \theta}=0; \tag{1}$$

radial momentum equation

$$\frac{1}{r}\frac{\partial r U_r^2}{\partial r}+\frac{\partial U_y U_r}{\partial y}+\frac{1}{r}\frac{\partial U_\theta U_r}{\partial \theta}-\frac{U_\theta^2}{r}$$
$$=-\frac{1}{\rho}\frac{\partial P}{\partial r}+\frac{2}{r}\frac{\partial}{\partial r}\left(r\nu_t\frac{\partial U_r}{\partial r}\right)+\frac{\partial}{\partial y}\left[\nu_t\left(\frac{\partial U_r}{\partial y}+\frac{\partial U_y}{\partial r}\right)\right]-\underline{\frac{2}{r^2}\nu_t U_r}; \tag{2}$$

vertical momentum equation

$$\frac{1}{r}\frac{\partial r U_r U_y}{\partial r}+\frac{\partial U_y^2}{\partial y}+\frac{1}{r}\frac{\partial U_\theta U_y}{\partial \theta}=-\frac{1}{\rho}\frac{\partial P}{\partial y}+\frac{1}{r}\frac{\partial}{\partial r}\left[r\nu_t\left(\frac{\partial U_r}{\partial y}+\frac{\partial U_y}{\partial r}\right)\right]+2\frac{\partial}{\partial y}\left(\nu_t\frac{\partial U_y}{\partial y}\right); \tag{3}$$

longitudinal momentum equation

$$\frac{1}{r}\frac{\partial r U_r U_\theta}{\partial r}+\frac{\partial U_y U_\theta}{\partial y}+\frac{1}{r}\frac{\partial U_\theta^2}{\partial \theta}+\frac{U_r U_\theta}{r}$$
$$=-\frac{1}{\rho}\frac{1}{r}\frac{\partial P}{\partial \theta}+\frac{1}{r}\frac{\partial}{\partial r}\left[r\nu_t\left(\frac{\partial U_\theta}{\partial r}-\underline{\frac{U_\theta}{r}}\right)\right]+\frac{\partial}{\partial y}\left(\nu_t\frac{\partial U_\theta}{\partial y}\right)+\underline{\frac{\nu_t}{r}\left(\frac{\partial U_\theta}{\partial r}-\frac{U_\theta}{r}\right)}; \tag{4}$$

concentration equation

$$\frac{1}{r}\frac{\partial r U_r C}{\partial r}+\frac{\partial U_y C}{\partial y}+\frac{1}{r}\frac{\partial U_\theta C}{\partial \theta}=\frac{1}{r}\frac{\partial}{\partial r}\left(\frac{\nu_t}{\sigma_C}r\frac{\partial C}{\partial r}\right)+\frac{\partial}{\partial y}\left(\frac{\nu_t}{\sigma_C}\frac{\partial C}{\partial y}\right). \tag{5}$$

The polar coordinate system is illustrated in figure 1 (*a*) where the symbols are also defined. In (2)–(5), the originally appearing turbulent stresses and mass fluxes were approximated by eddy viscosity and diffusivity relations respectively. σ_C is the turbulent Schmidt number for the pollutant concentration, which represents the ratio of eddy viscosity ν_t to eddy diffusivity Γ_t. A value of $\sigma_C = 0.5$ has been found suitable in previous calculations of pollutant spreading in open-channel situations (Rastogi & Rodi 1978; Rodi, Pavlovic & Srivatsa 1981) and is used in this study. The molecular diffusion terms have been neglected in the above equations because these are integrated only in the fully turbulent regions outside the viscous sublayer. This layer is bridged by empirical wall functions which will be introduced below in the section on boundary conditions.

Shear-layer approximations have been introduced to eliminate the terms expressing diffusivity (turbulent) transport of momentum and mass in the streamwise direction, i.e. all diffusion terms involving gradients of θ have been neglected. This simplification is justified in shear-layer flows with a predominant flow direction, which restricts the present analysis to flows without separation. The omission of the streamwise diffusion terms has important consequences for the numerical solution procedure. By this omission, the equations assume a 'parabolic' character, i.e. changes in

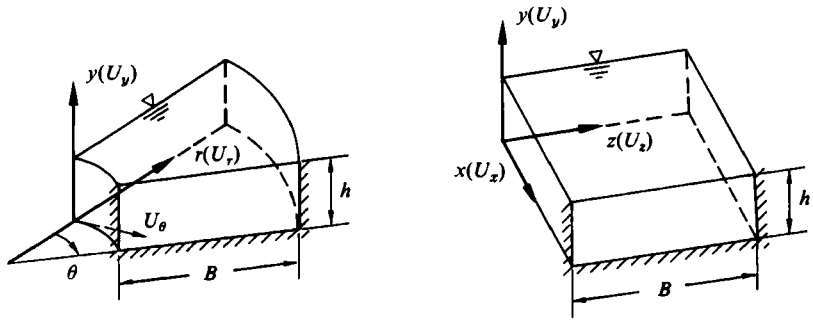

FIGURE 1. Coordinate systems: (*a*) cylindrical polar, (*b*) Cartesian.

the dependent variables at downstream positions cannot be transmitted to upstream locations by convection or diffusion. It must be emphasized however that the highly important downstream-to-upstream linkage due to surface-elevation changes is retained because this linkage is represented by the coupling of (4) to (2) and (3) via the pressure. The elliptic character of the pressure relations is therefore retained, as is discussed in greater detail in Leschziner & Rodi (1979). Therefore the momentum equations (2)–(4) are only partially parabolic, while the concentration equation (5) is fully parabolic. The latter can therefore be solved by a very economical once-through forward-marching integration, while the momentum equations, together with the continuity equation, require a 'repeated forward-marching solution', which is still more economical than an iterative solution necessary for fully elliptic equations.

The governing equations for the straight sections are obtained from (1)–(5) by setting the underlined terms to zero and the radius r to unity in all the other terms. The system $(r, y, \theta, U_r, U_y, U_\theta)$ then reverts to the Cartesian system (x, y, z, U_x, U_y, U_z) illustrated in figure 1 (*b*).

2.2. *Turbulence model*

The distribution of the eddy viscosity ν_t appearing in (2)–(5) is determined using the k–ϵ turbulence model described in detail by Launder & Spalding (1974). This relates ν_t to the turbulent kinetic energy k, and to the rate of its dissipation ϵ, by

$$\nu_t = c_\mu \frac{k^2}{\epsilon}, \tag{6}$$

where c_μ is an empirical constant. The distribution of k and ϵ is obtained by the solution of modelled transport equations for these quantities, which read in the polar coordinate system:

$$\frac{1}{r}\frac{\partial r U_r k}{\partial r} + \frac{\partial U_y k}{\partial y} + \frac{1}{r}\frac{\partial U_\theta k}{\partial \theta} = \frac{1}{r}\frac{\partial}{\partial r}\left(\frac{\nu_t}{\sigma_k} r \frac{\partial k}{\partial r}\right) + \frac{\partial}{\partial y}\left(\frac{\nu_t}{\sigma_k}\frac{\partial k}{\partial y}\right) + G - \epsilon; \tag{7}$$

$$\frac{1}{r}\frac{\partial r U_r \epsilon}{\partial r} + \frac{\partial U_y \epsilon}{\partial y} + \frac{1}{r}\frac{\partial U_\theta \epsilon}{\partial \theta} = \frac{1}{r}\frac{\partial}{\partial r}\left(\frac{\nu_t}{\sigma_\epsilon} r \frac{\partial \epsilon}{\partial r}\right) + \frac{\partial}{\partial y}\left(\frac{\nu_t}{\sigma_\epsilon}\frac{\partial \epsilon}{\partial y}\right) + c_{\epsilon 1}\frac{\epsilon}{k} G - c_{\epsilon 2}\frac{\epsilon^2}{k}; \tag{8}$$

where

$$G = \nu_t \left\{ 2\left[\left(\frac{\partial U_r}{\partial r}\right)^2 + \left(\frac{\partial U_y}{\partial y}\right)^2 + \underline{\left(\frac{U_r}{r}\right)^2}\right] + \left(\frac{\partial U_r}{\partial y} + \frac{\partial U_y}{\partial r}\right)^2 + \left(\frac{\partial U_\theta}{\partial y}\right)^2 + \left[r \frac{\partial}{\partial r}\left(\frac{U_r}{r}\right)\right]^2 \right\} \tag{9}$$

is the rate of production of turbulent kinetic energy by the interaction of mean-velocity gradients and turbulent stresses. Standard values of the empirical constants have been taken from Rodi (1980): $c_\mu = 0.09$, $c_{\varepsilon 1} = 1.44$, $c_{\varepsilon 2} = 1.92$, $\sigma_k = 1$, $\sigma_\varepsilon = 1.3$. By omitting the underlined term and equating the radius r to unity, the turbulence model equations (7)–(9) also revert to those of the Cartesian system used in the straight channel sections.

In the above turbulence model, the effects of curvature on the turbulence are accounted for only by terms arising from the transformation of the model equations into polar coordinates. Rodi & Scheuerer (1983) have shown that this model does not adequately simulate the influence of curvature on turbulence that has been observed in boundary layers developing along curved walls. The effect is generally to decrease the turbulent mixing in flow along convex walls and to increase it on concave ones. Bradshaw (1973) has given a comprehensive description of these phenomena and has shown the close analogy to the influence of buoyancy on turbulence in atmospheric boundary layers. In order to account properly for the extra curvature effects, a higher-level turbulence model is necessary such as the Reynolds-stress-equation model of Launder, Reece & Rodi (1975) or a simplified algebraic-stress derivative of it. The Launder, Reece & Rodi model was applied by Gibson & Rodi (1981) to strongly curved mixing layers and an algebraic-stress-model version was used by Rodi & Scheuerer (1983) to calculate various two-dimensional curved shear layers (wall boundary layers, mixing layers and wall jets). In these curved-flow examples, pressure gradients played an insignificant role and the flow development was governed mainly by the turbulent shear stresses. However, in channel flows with strong curvature such as those considered here, the pressure gradients are in most parts considerably larger than the gradients of the Reynolds stresses so that refined modelling of these stresses appearing in the momentum equations is not really necessary. On the other hand, the concentration equation does not contain a pressure-gradient term so that the pollutant concentration field is more strongly influenced by effects of curvature on turbulent mixing and hence by the modelling of these effects. Thus, it is considered sufficient for the present purpose to introduce a relatively simply modification to the eddy diffusivity appearing in the concentration equation. The approach followed is to assume that ν_t in the vertical diffusion term in (5) (second term on the right-hand side) is determined in the usual way by (6) with a standard value of $c_\mu = 0.09$, but that ν_t in the transverse diffusion term (first term on the right-hand side) has a variable c_μ given by

$$c_{\mu,r} = \frac{0.09}{1+0.57\dfrac{k^2}{\varepsilon^2}\left(\dfrac{\partial U_s}{\partial n}+\dfrac{U_s}{R}\right)\dfrac{U_s}{R}}. \tag{10}$$

Here, U_s is the resultant horizontal velocity, n is the distance in the direction normal to it and R is the local radius of curvature of the streamlines. This expression was derived by Leschziner & Rodi (1981) for two-dimensional flows with streamline curvature, based on the algebraic-stress-model proposed by Gibson (1978). This model assumes that turbulence is in a state of local equilibrium so that convection and diffusion terms in the Reynolds-stress equations can be neglected. In the calculations reported below, relation (10) led to $c_{\mu,r}$ values as low as 0.01 and as high as 0.9 at isolated points.

Equation (10) could be simplified further by replacing U_s by the longitudinal velocity component U_θ and R by the radius of curvature r of the longitudinal grid line at the location considered since the radial velocity component is usually less than

10% of the longitudinal one in the cases considered. However, it was necessary to allow for a smooth transition of the value of R in curved and straight sections.

2.3. *Solution procedure and boundary conditions*

As mentioned above, the flow field is governed by partially parabolic, and the concentration field by fully parabolic, differential equations. Thus, an efficient, repeated-forward-marching solution procedure can be employed which repeatedly covers the calculation domain, starting from given conditions at the initial cross-section and a guessed three-dimensional pressure distribution. The pressure distribution is updated with each iteration until convergence is attained. All the other variables require only two-dimensional storage. Since, for the non-buoyant situations considered here, the pollutant concentration has no influence on the flow field, a converged solution is first obtained for the velocity and pressure fields. The velocity field is then stored for the subsequent computation of the pollutant concentration distributions for various discharge situations. As the concentration equation is fully parabolic, each calculation requires only one additional sweep. The solution procedure is a modified version of the partially parabolic procedure of Pratap & Spalding (1976) which itself is an extension of the parabolic procedure of Patankar & Spalding (1972). For the calculation of the flow in the channel with a single meander, the conditions at the initial cross-section are prescribed as uniform with the experimental values, while for the channel with a series of meanders, periodic conditions are employed. Thus, the exit conditions for one iteration are used as initial conditions for the next, until both conditions do not change any more from iteration to iteration. This applies of course only for the flow field as the concentration behaviour is not periodic. In order to calculate the pollutant spreading in such a case, the individual meander reaches (all having the same velocity field) are covered one after the other by single sweeps, the exit conditions resulting from the solution for one reach then representing the initial conditions for the calculation of the next reach.

Boundary conditions need to be prescribed at the solid walls (bed and banks) and at the free surface for all dependent variables. In the present model, the surface is treated as a 'rigid lid' so that the generally non-planar surface is replaced by a fictitious, frictionless plane surface parallel to the channel bed. This boundary is then assumed to behave as a plane of symmetry with the velocity component normal to it and the normal gradients of all other quantities equal to zero. It is important to emphasize that the surface-elevation changes are not neglected by implementing this approximation, but are accounted for implicitly by the non-zero pressure gradients $\partial P/\partial r$ and $\partial P/\partial \theta$ at the rigid lid. The transverse and longitudinal surface slopes may be computed from these as

$$\frac{\partial h}{\partial r} = \frac{1}{\rho g}\left(\frac{\partial P}{\partial r}\right)_s; \quad \frac{\partial h}{\partial \theta} = \frac{1}{\rho g}\left(\frac{\partial P}{\partial \theta}\right)_s. \tag{11}$$

It should be noted however that there is a continuity error accompanying this treatment of the free surface. As was shown by McGuirk & Rodi (1977), this error is small when the superelevation is less than about 10% of the channel depth. This is invariably the case for the flows considered here.

At solid walls, the velocity normal to the wall is set to zero; otherwise the wall-function approach outlined by Launder & Spalding (1974) is adopted. According to this, the boundary conditions are not specified right at the wall but at a point outside the viscous sublayer where the logarithmic law of the wall prevails and turbulence can be assumed to be approximately in a state of local equilibrium. For

such a point at a distance y from the wall, the velocity component parallel to the surface is related to the friction velocity U_τ as

$$U_w = U_\tau \frac{1}{\kappa} \ln (Ey^+) \cos\phi, \tag{12}$$

where $y^+ = U_\tau y/\nu$ and should lie in the range 30–100. ϕ is the angle between the directions of the velocity component and the resultant friction velocity, κ is the von Kármán constant (here 0.42) and E is a roughness parameter which is given a value of 9.0 for smooth walls and lower values for rough walls. The boundary conditions for k and ϵ are also specified at the first grid point at a distance y from the wall where the logarithmic law of the wall prevails. With this and the assumption of local equilibrium there follows

$$k_w = \frac{U_\tau^2}{c_\mu^{\frac{1}{2}}}; \quad \epsilon_w = \frac{U_\tau^3}{\kappa y}. \tag{13}$$

The flux of pollutants at walls is zero so that the concentration gradients normal to walls are prescribed as zero. No direct boundary conditions are required for the pressure since the velocity normal to the wall is zero, which implies zero pressure gradient in that direction. The boundary conditions for the initial cross-section have been discussed already, but in the experiments simulated here the pollutant was usually discharged through a small tube downstream of the initial plane of the calculation domain. The plane coinciding with the point of discharge forms the initial plane for the calculation of the pollutant concentration. There the concentration is prescribed as uniform within the control volume surrounding the grid node coincident with the injection port and zero everywhere else in the cross-section. The linear dimensions of the injection control volume are typically five times as large as those of the actual port openings in the experiments, but as the presence of the injection tube is expected to produce considerable turbulence near the discharge location the injected dye probably mixes very quickly with the channel water. Therefore, the idealized representation of the discharge port by a control-volume area much larger than the actual discharge area did not introduce any drastic errors. However, the initial mixing is certainly not simulated very accurately. Some trial calculations were made using exponential profiles some distance after the discharge to introduce the pollutant into the flow, as would apply in the case of a point discharge into a uniform stream (see Fischer *et al.* 1979), but this practice gave worse results than the one described above. The reason for this is that the secondary motion at the discharge location led to skewing of the pollutant concentration field very close to the discharge, which the present method approximates, but which is neglected when exponential profiles are used. The skewing effect appears to be of some importance to the subsequent concentration-field development.

Because of the parabolic nature of the differential equations, except for the influence of the pressure, boundary conditions are required at the outflow plane only for the pressure. For this quantity, the second streamwise derivative is set to zero at the outflow boundary.

3. Results and discussion

3.1. *Test cases considered*

The mathematical model described above is applied to predict the three-dimensional flow and concentration fields in the meandering channels with rectangular cross-

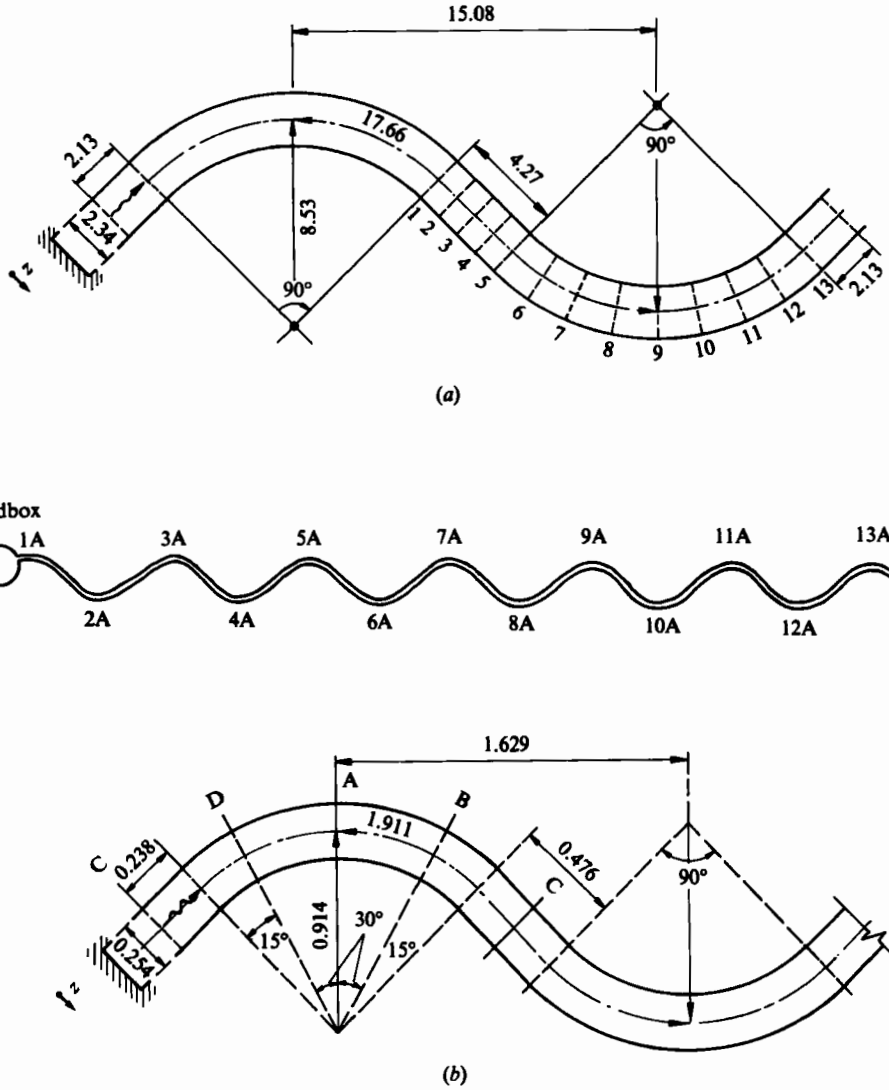

FIGURE 2. Flow configurations computed (all distances in m). (*a*) Case 1; experimental data by Chang (1971); (*b*) cases 2 and 3; experimental data by Chang (1971) and Fukuoka (1971).

section studied experimentally by Chang (1971) and Fukuoka (1971). The two configurations are illustrated in figure 2(*a*, *b*). The details of the experimental conditions are summarized in table 1.

The case-1 experiments were carried out in a large flume (width $B = 2.34$ m) with only a single meander while the experiments for cases 2 and 3 were performed in a small flume ($B = 0.254$ m) with 7 meanders. In cases 1 and 2, all channel walls were nominally smooth, while in case 3 the bed was rough and only the sidewalls were nominally smooth. In the computations, the value of the roughness parameters E in the logarithmic law of the wall (12) was adjusted through trial and error such that the same friction factor f resulted as in the experiments with the smooth walls. A value of 3.0 was found for case 1 and a value of 3.7 for case 2. The latter was employed also for the 'smooth' sidewalls in case 3, and the value of E for the rough bed was

Case	Depth h (m)	Width-to-depth ratio B/h	Mean radius-to-width ratio R_c/B	Bulk velocity $\bar{U}$ (m/s)	Reynolds number ($\times 10^3$) $= \frac{\rho \bar{U} D_h}{\mu}$	Friction factor $f = 8\left(\frac{U^*}{\bar{U}}\right)^2$	Froude number $\frac{U}{(gh)^{\frac{1}{2}}}$	Comments
Case 1 (smooth bed)	0.115	20.3	3.66	0.366	181	0.0215	0.345	Single meander; velocity and concentration fields by Chang (1971)
Case 2 (smooth bed)	0.057	4.48	3.60	0.354	40	0.0293	0.473	Series of meanders; velocity field by Fukuoka (1971), concentration field by Chang (1971)
Case 3 rough) bed)	0.054	4.68	3.60	0.205	25	0.0930	0.275	

TABLE 1. Experimental conditions for meandering channels

then adjusted to obtain the experimental friction factor. This value is 0.05. It should be noted that both laboratory flumes have a sinuosity (ratio of straight-line slope to actual channel slope) of 1.17 which corresponds to sinuous rivers (sinuosity less than 1.5) rather than meandering rivers according to the classification of Leopold & Wolman (1957). However, as has been observed by De Vriend (1981*b*), channels with rectangular cross-sections have much stronger lateral dispersion than those with mildly sloping banks occurring in natural rivers. Thus, the experiments considered here have pollutant dispersions comparable with those in rivers with much higher sinuosities. Of course, meandering channels formed by 90° bends in alternate directions can only have sinuosities in the range 1.111–1.414. In order to obtain higher values, the bends must subtend larger angles. In cases 1 and 2, three separate experimental runs were carried out to study the pollutant dispersion. The pollutant (Rhodamin B dye) was introduced at three locations, namely near the inner bank, at the outer bank and at the mid-plane, each at mid-depth. In case 3, only injections at the inner and outer bank were studied.

3.2. *Computational details*

The computations were performed, in each case, on a grid with 14 nodes in the vertical, 24 nodes in the transverse and 122 nodes in the longitudinal direction. Of the latter, 8 nodes were placed in each of the inlet and outlet tangents, 46 nodes in each curved section and 14 nodes in the straight middle tangent. The calculations were found to be highly sensitive to the grid resolution in the longitudinal direction, especially in the curved sections. The values quoted above for the grid distribution have been found optimal, achieving reasonable accuracy without excessive computational cost. Calculations with a grid twice as fine did not produce appreciably different results, but this does not really demonstrate that the results are fully grid-independent. The computational requirements were, on the average, 780 Kbytes of main core memory and 20 s per iteration on a Siemens 7880 computer. 60 iterations were required for convergence of the main flow field. The pollutant concentration fields were then obtained with a final single sweep.

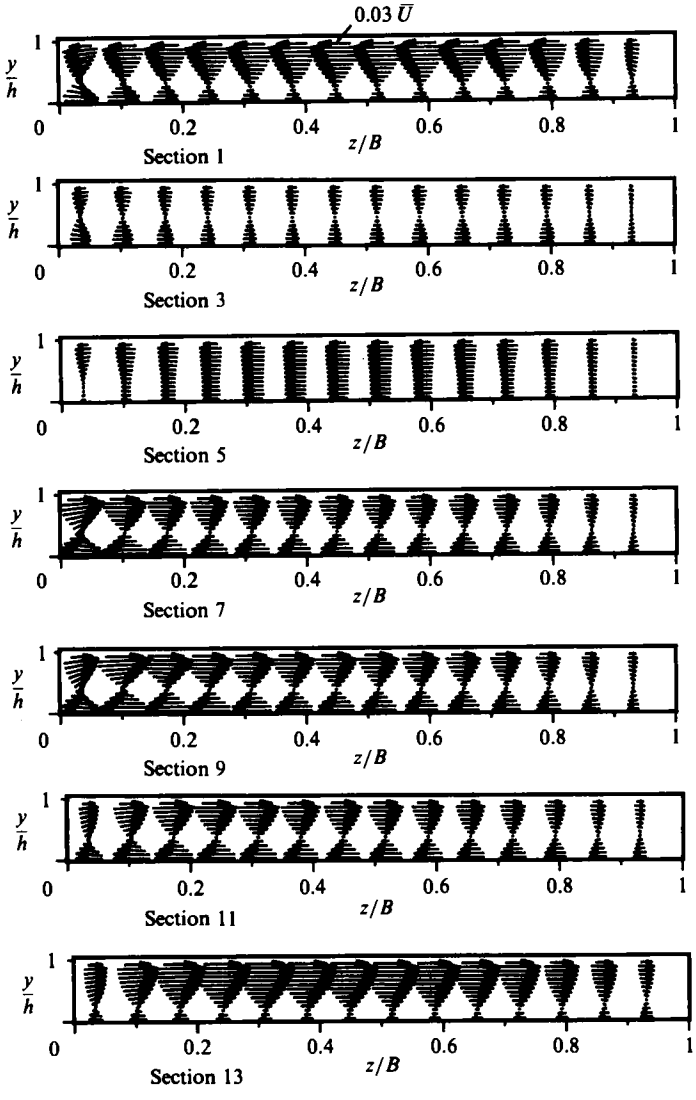

FIGURE 3. Computed velocity vectors in cross-stream planes, case 1.

3.3. *Comparison of predictions with experiments*

3.3.1. *Flow field*

Figure 3 shows the computed secondary velocity vector for case 1 at 7 cross-sections between the end of the first bend and the end of the second bend. The location of the individual sections can be seen from figure 2(*a*). The realism of the predictions can be checked with the aid of figure 4 where the vertical profiles of the radial velocity component are compared with the measurements of Chang (1971) at selected cross-sections. At the end of the first bend (section 1), figures 3 and 4 show a strong secondary motion near the water surface from the inner to the outer bank, accompanied by a weaker counterflow near the bed. As can be seen from figure 4(*a*), the predictions agree quite well with the measurements at this cross-section, except for the failure of the model to predict what appears to be a small counter-rotating

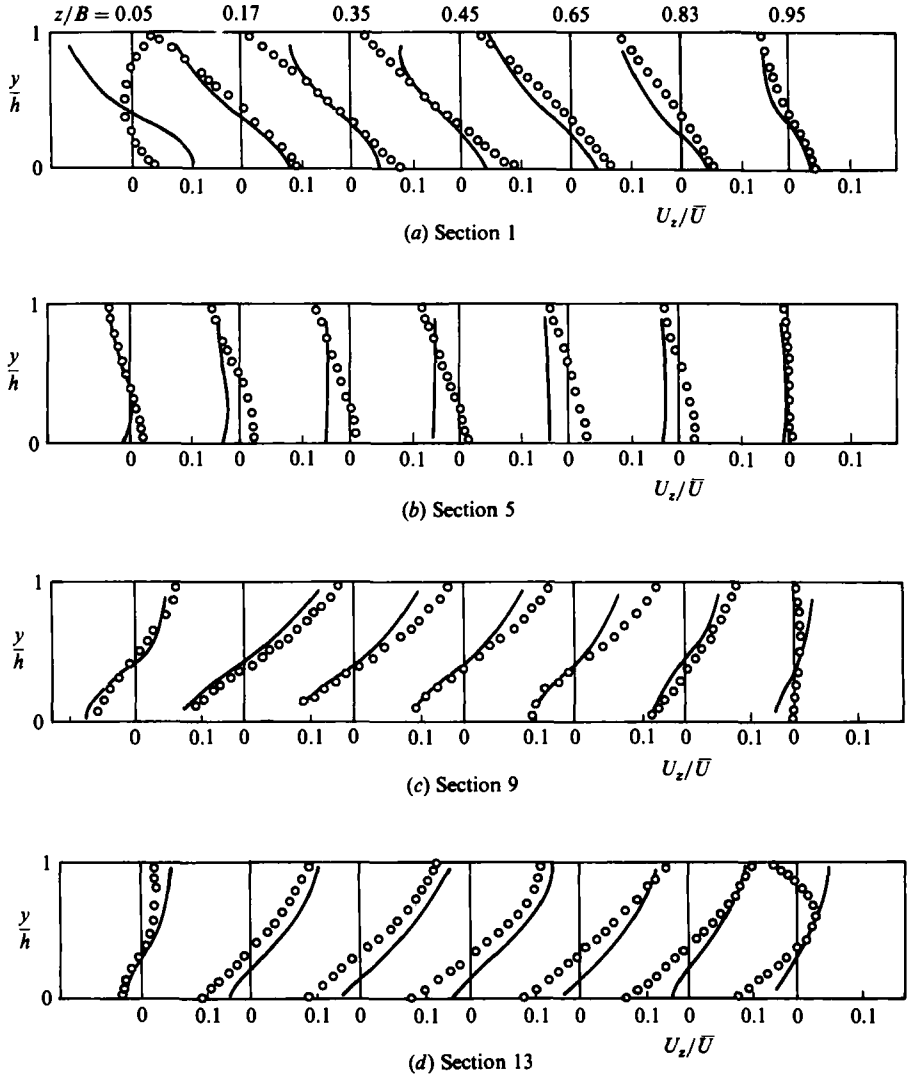

FIGURE 4. Comparison of lateral velocity profiles, case 1: ——, predictions; OOO, measurements (Chang 1971).

vortex near the top corner of the outer bank. At the middle of the tangent between the bends (section 3), the inward and outward motions appear to be of equal strength and reduced magnitude, indicating the decay of the secondary motion in the straight section. At the entrance to the second bend (section 5) there is no spiral motion but a unidirectional, radially inward motion. This is caused by the longitudinal acceleration and deceleration of the fluid at the inner and outer bank respectively, which, for reasons of continuity, causes the fluid to move from the outer to the inner regions. According to the comparison with measurements shown in figure 4(b), this process seems to be overpredicted. Inside the bend (section 7) a spiral motion develops which counter-rotates to that in the previous bend. The strength of the secondary motion is increased all the way through the bend; at the end of the bend (section 13) there is again a strong motion from the inner to the outer bank near

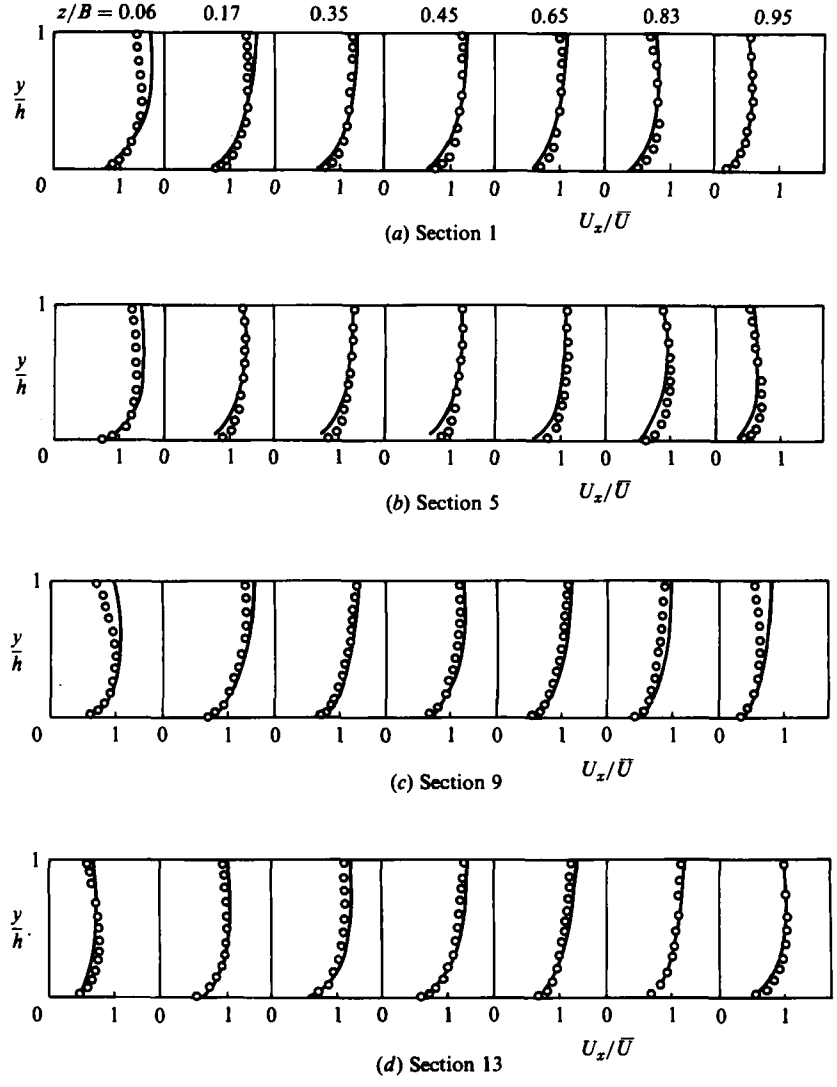

FIGURE 5. Comparison of longitudinal velocity profiles, case 1: ——, predictions, ○○○, measurements (Chang 1971).

the surface and a significantly weaker counterflow near the bed. Here also, the measurements indicate a counter-rotating vortex near the top of the outer bank. This is again not reproduced by the calculation, perhaps because of insufficient numerical resolution and also because the turbulence model employed is rather crude for resolving such near-wall details of the flow. Otherwise, the secondary motion is simulated very well at sections 9 and 13 so that, overall, the development of the secondary flow is predicted with acceptable accuracy.

For case 1, the vertical profiles of the longitudinal velocity component are compared with measurements in figure 5. The agreement can be seen to be generally fairly good. The bulging of the velocity profiles near the sidewalls representing a depression of the velocity maximum below the surface is reasonably well reproduced except perhaps at section 9. This bulging is due to the secondary motion convecting

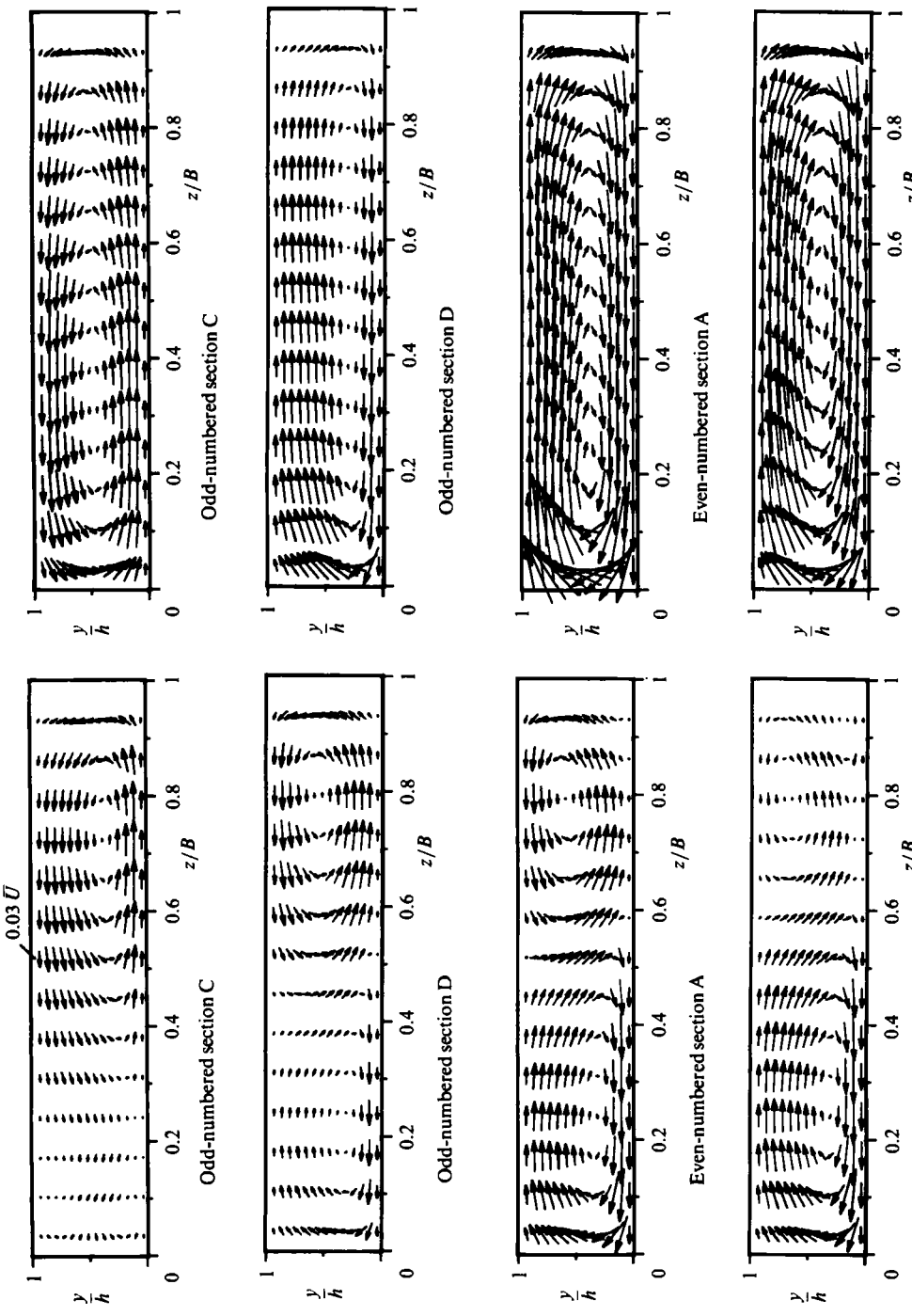

(a) Case 2 (b) Case 3

FIGURE 6. Computed velocity vectors in cross-stream planes, cases 2 and 3.

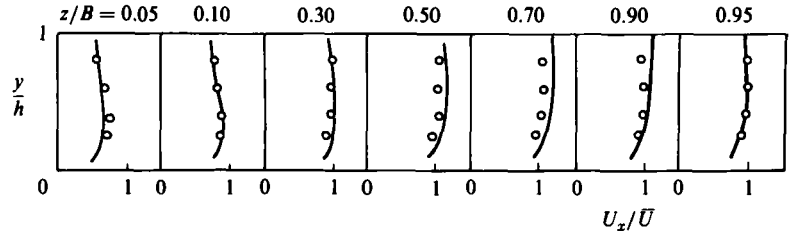

(*a*) Even-numbered section C

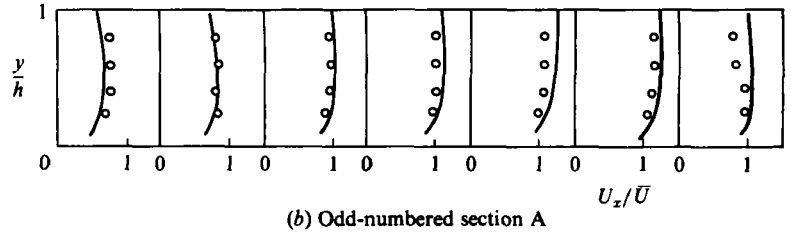

(*b*) Odd-numbered section A

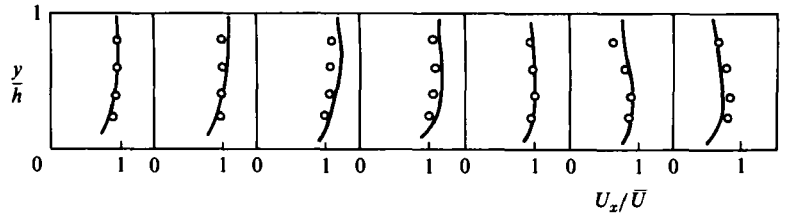

(*c*) Odd-numbered section C

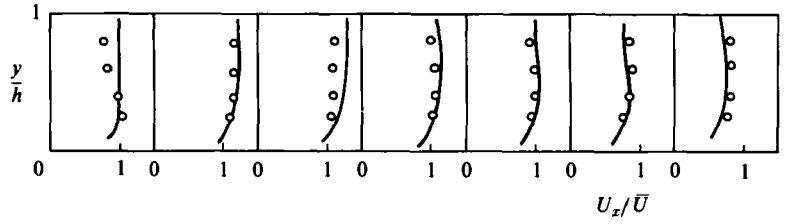

(*d*) Even-numbered section A

FIGURE 7. Comparison of longitudinal velocity profiles, case 2: ——, predictions, ○○○, measurements (Fukuoka 1971).

high-momentum fluid from the surface to regions below the surface. The shifting of the low-velocity region from the outer bank to the inner bank between the middle (section 9) and the end (section 13) of the second bend is also quite well predicted.

Figure 6 shows the computed velocity vectors for cases 2 and 3 at various sections covering one complete meander. In each case the flow is periodic so that the picture repeats itself for the subsequent meander. Secondary velocity measurements are unfortunately not available for these cases. The channel has an aspect ratio of 4.48, which is much lower than that of the channel of case 1 (20.3). Accordingly, in case 2 (figure 6*a*) the secondary flow field is very different even though the bed and

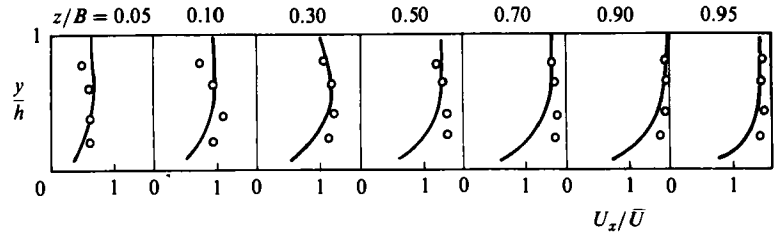

(*a*) Even-numbered section C

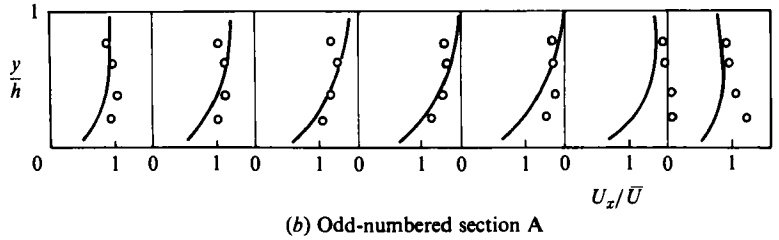

(*b*) Odd-numbered section A

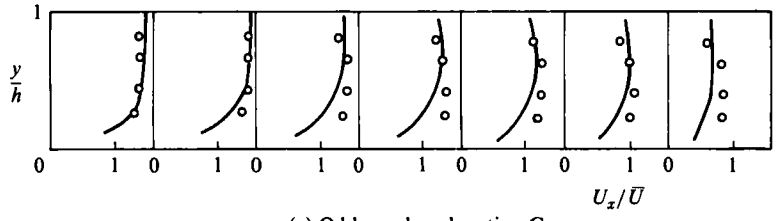

(*c*) Odd-numbered section C

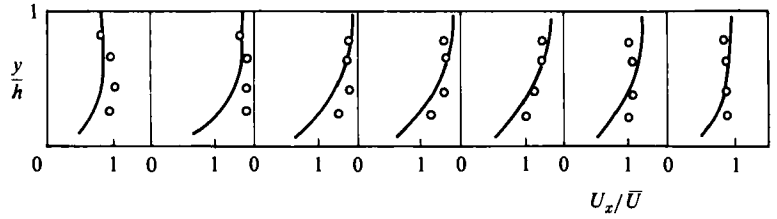

(*d*) Even-numbered section A

FIGURE 8. Comparison of longitudinal velocity profiles, case 3: ——, predictions, ○○○, measurements (Fukuoka 1971).

sidewalls were also nominally smooth. At each cross-section, there are two fairly large eddies present and there appears to be a continuous exchange of fluid between the two eddies, with the situation reversing from one bend to the other. Towards the end of each bend, (sections B and C) one eddy dominates the other and this has the same sense of rotation as in the previous case 1 (i.e. outward motion near the surface and inward motion near the bed). Among others, Tamai *et al.* (1983) observed in their experiment in a channel with a single meander consisting of two alternate 90° bends connected by a short tangent that, for $R_c/B = 2.0$ and $B/h = 10$, there existed two counter-rotating eddies at each cross-section which appeared to exchange fluid with one another as the flow proceeded round the bend. However, their schematic representation of these eddies showed them as lying one above the other rather than

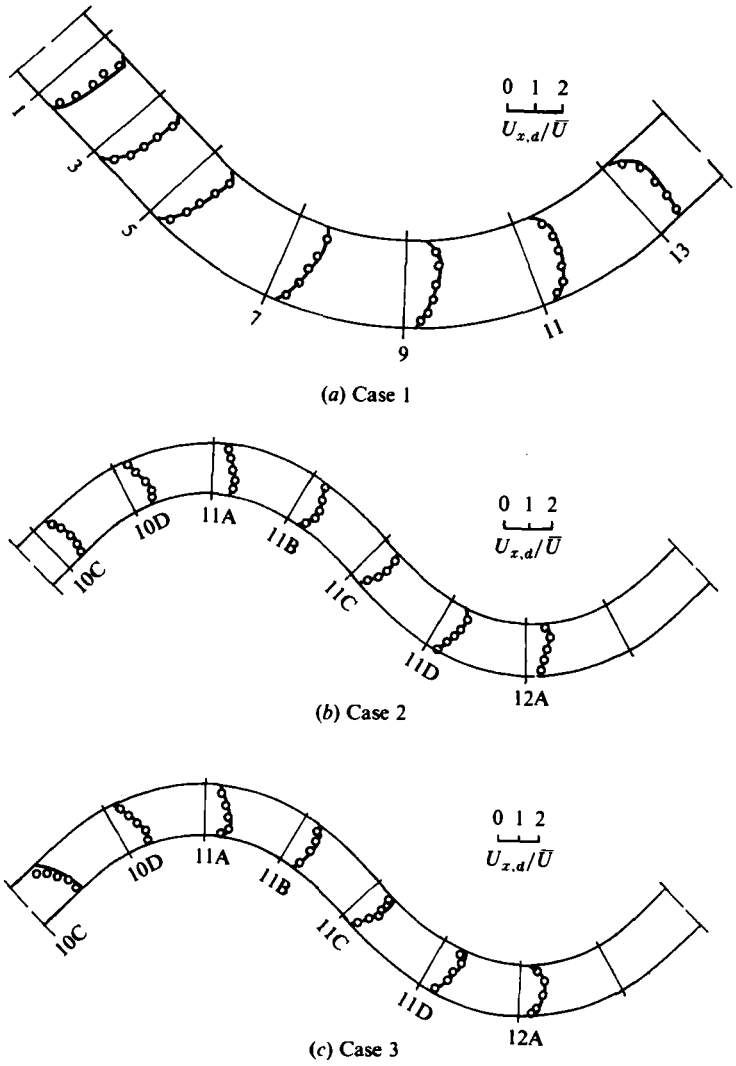

FIGURE 9. Comparison of depth-averaged longitudinal velocity profiles: ——, predictions; OOO, measurements Chang (1971).

side by side as in the present calculation. In case 3, with smooth walls but a rough bed there exists only a single eddy at most cross-sections, with the secondary flow pattern very similar to that of case 1, in spite of the much smaller aspect ratio (4.68 cf. 20.3). The strength of the spiral motion is also larger ($U_\tau/U \approx 0.3$) than for case 2 ($U_\tau/U \approx 0.15$) with a smooth bed. It appears that the bed roughness has a dominant effect on the secondary flow pattern in that it stabilizes the formation of a single eddy, which in turn increases the magnitude of the secondary motion. The predicted and measured vertical profiles of the longitudinal velocity component are compared for case 2 in figure 7. The agreement is largely satisfactory. The bulging is again reproduced correctly for most profiles. Similar comparisons are shown in figure 8 for case 3, in which the channel has a rough bed and smooth sidewalls. The agreement between predictions and measurements is now not so good. The predicted

velocity profiles are typical of rough-bed channel flow, with some skewing caused by the secondary motion. On the other hand, the measured profiles are in most cases nearly uniform in the vertical direction, with some deviations which may again be due to the secondary flow. Such profiles are rather atypical for flow in straight, shallow channels with a rough bed. A possible explanation for this behaviour would be that the secondary motion generated in the channel was so strong that it distorted highly the typical rough-bed velocity profiles. As the secondary velocities were not measured in this case this explanation must remain speculative. The measured velocity profiles can be noted to be not completely periodical as the antisymmetry, which should exist between odd- and even-numbered sections, is not always reflected in the profiles. This casts some doubt on the accuracy of the measurements. On the other hand, Fukuoka & Sayre (1973) state that the velocity measurements obtained with a 1.6 mm diameter Prandtl Pitot tube connected to a 1.0 kN/m^2 Statham pressure cell should be accurate to within 10% for velocities as low as 0.25 $\bar{U}$ for the case under consideration. The differences between the predicted and measured velocity profiles remain therefore somewhat puzzling.

Finally, predicted and measured depth-averaged velocity profiles at various cross-sections are compared for all three cases in figure 9. As has been discussed in §1, the velocity maximum is near the inner bank at the entrance of the bend and then moves to the outer bank towards the exit. There is generally good agreement for this development between calculations and measurements in all three cases. The measurements indicate that the lateral velocity profiles are less uniform in case 3 with a rough bed than in case 2 with a smooth bed, which is accompanied by a stronger shift of the velocity maximum. This behaviour points to differences in the development of the secondary motion and the trend is reproduced quite well by the model in spite of the differences experienced with the vertical profiles.

3.3.2. *Concentration field*

The predictions of the pollutant concentration distributions are compared with the measurements of Chang (1971) in figures 10–12 for the three test cases. The dye injection points are indicated in each of the figures. In case 1 (figure 10) the dye was injected in the first quarter of the first bend and the development of the ensuing concentration field is shown for the second bend. In cases 2 and 3 with altogether seven meanders, the dye was injected at cross-section 8C and the concentration development was calculated up to cross-section 12A. In each of cases 1 and 2, three runs were made with the pollutant injected at the inner bank, the outer bank and at the centre of the channels as indicated in figures 10 and 11. In case 3 only the two injections at the inner and outer bank, for which measurements were carried out, were simulated. The figures present the development of the depth-averaged concentration profiles that are of greatest practical significance. The measured depth-averaged profiles are based on measurements at four depths at each location. The computed results represent the average over the 12 internal grid nodes in the vertical direction. All computations were carried out with both a constant value of c_μ and with variable $c_{\mu,r}$ according to (10). However, appreciable differences between the two sets of predictions can be discerned only for the discharges at the outer bank and in the centre of case 2, as shown in figure 11 (a, b). These differences may be explained as follows. The curvature correction mimics the destabilizing effect of boundary-layer flow along concave walls and the stabilizing effect of flow along convex walls by increasing the eddy diffusivity along the former and decreasing it along the latter. This appears to have a significant effect on the concentration

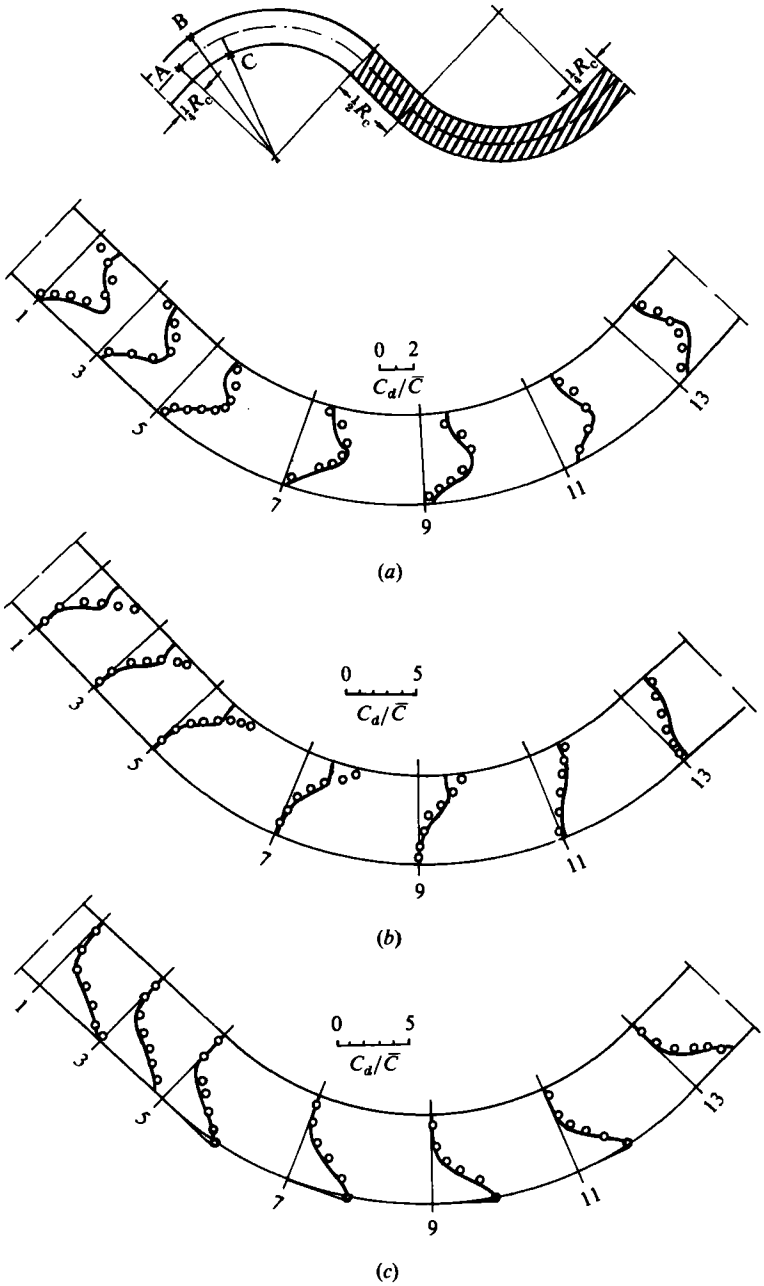

FIGURE 10. Comparison of depth-averaged concentration profiles, case 1: ——, predictions; ○○○, measurements (Chang 1971): (*a*) Dye at A; (*b*) dye at B; (*c*) dye at C.

distribution only in the channel with relatively low aspect ratio and smooth bed (case 2). In case 1 the aspect ratio is rather high (≈ 20) so that the turbulence in most parts of the channel is probably dominated by the bed shear stress and not by the boundary layers of the sidewalls, the only regions where curvature effects can play a role. In case 3, in spite of the relatively low aspect ratio, the turbulence is again generated mainly by the bed shear stress because this is rather high owing to the

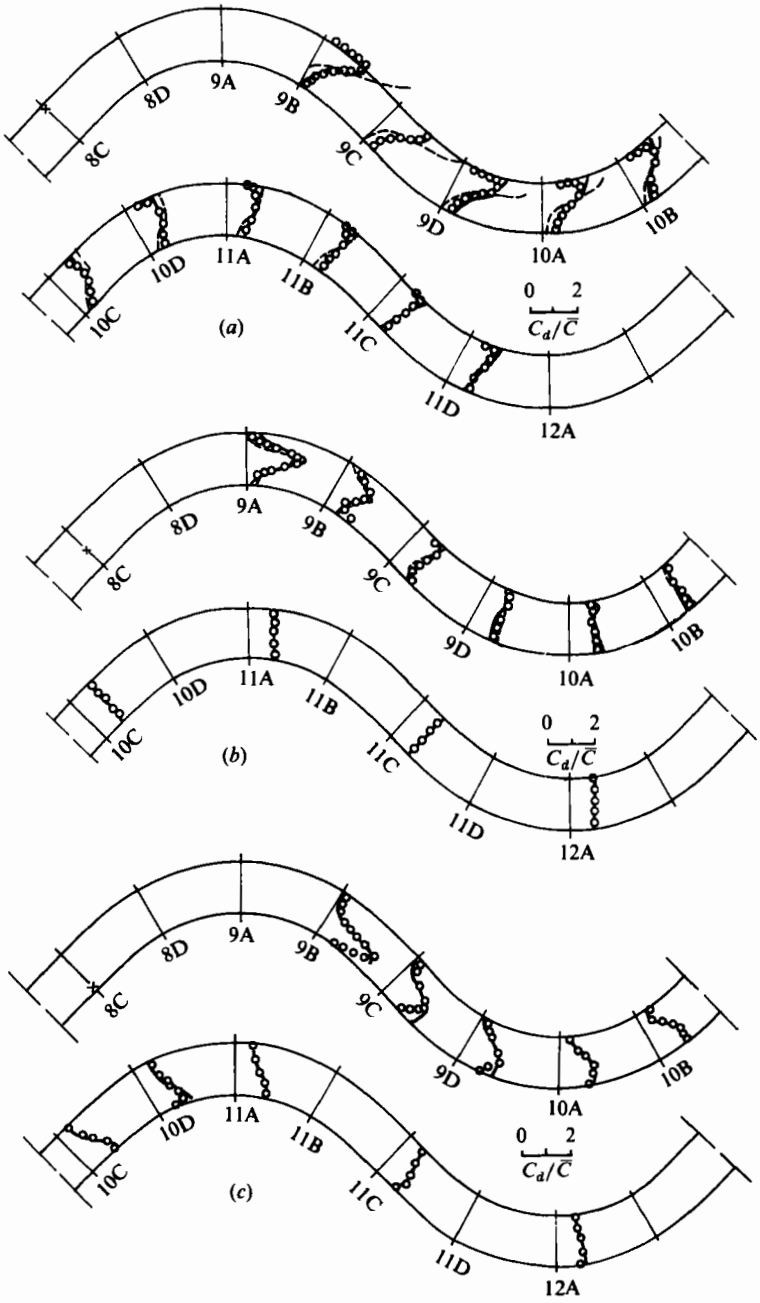

FIGURE 11. Comparison of depth-averaged concentration profiles, case 2: ○○○, measurements (Chang 1971); ——, predictions $C_{\mu,r}$ from equation (10); – – –, predictions $C_{\mu,r} = C_\mu = 0.09$. (*a*) Outer-bank discharge; (*b*) central discharge; (*c*) inner-bank discharge.

rough bed. In fact, the turbulence level in this case is considerably higher than in case 2. Further, due to the dominating influence of the bed on the turbulence generation, curvature effects acting on the sidewall boundary layers can have little influence on the diffusivity in this case. Also for the discharge at the inner bank in case 2, the curvature correction has little effect. In this discharge situation, the

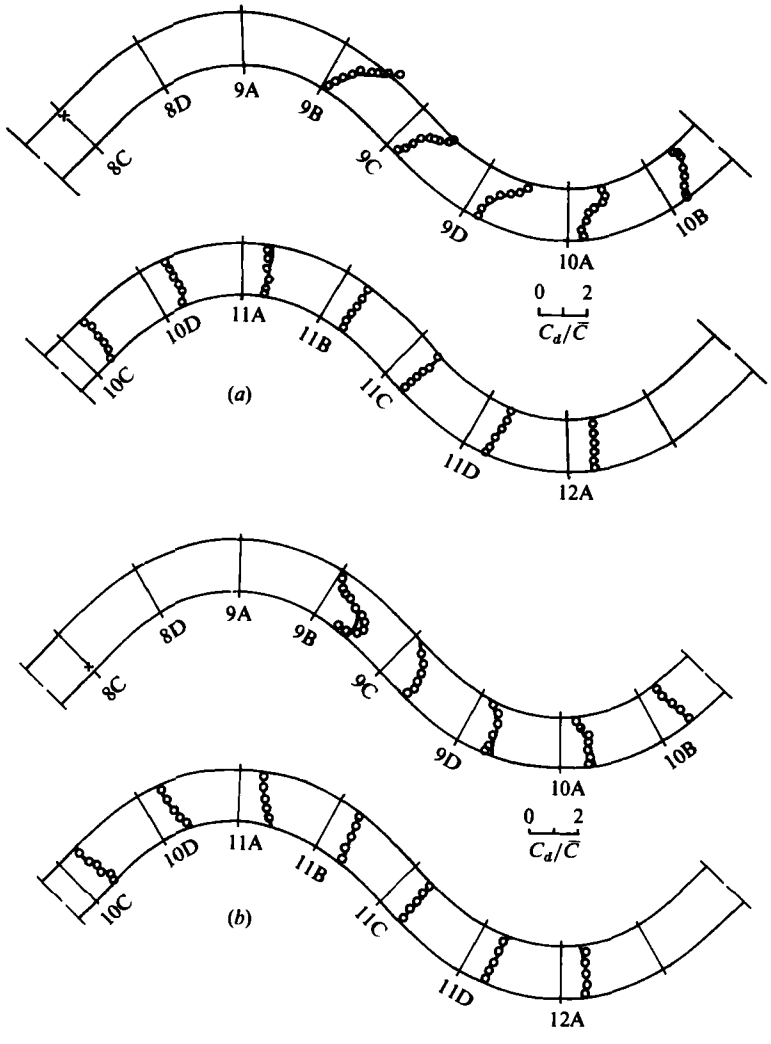

FIGURE 12. Comparison of depth-averaged concentration profiles, case 3: ○○○, measurements (Chang 1971); ——, predictions. (*a*) Outer-bank discharge; (*b*) inner-bank discharge.

injected dye moves first along a convexly curved wall (section 8C–9C) where the curvature effect is to reduce the diffusivity generated by the inner bank. The low values of the diffusivity that would result here are again overruled by the turbulence generated near the bed so that the curvature correction does in fact not become effective. It is clear from figure 11 (*a*, *b*) that the curvature correction is in the right direction so that the profiles obtained with this correction agree much better with the measured profiles than those obtained with a constant c_μ value.

The predicted depth-averaged concentration profiles show fairly good agreement with the measurements in the large meandering flume (case 1) as shown in figure 10. The largest discrepancies appear near the inner bank of the test section for the discharge being placed at the outer bank (at point B). The deviation had probably already developed very near the discharge and merely propagates downstream. The difficulty in simulating correctly the actual situation near the discharge port has been mentioned previously. For case 2, with the discharge at the outer bank (figure 11*a*)

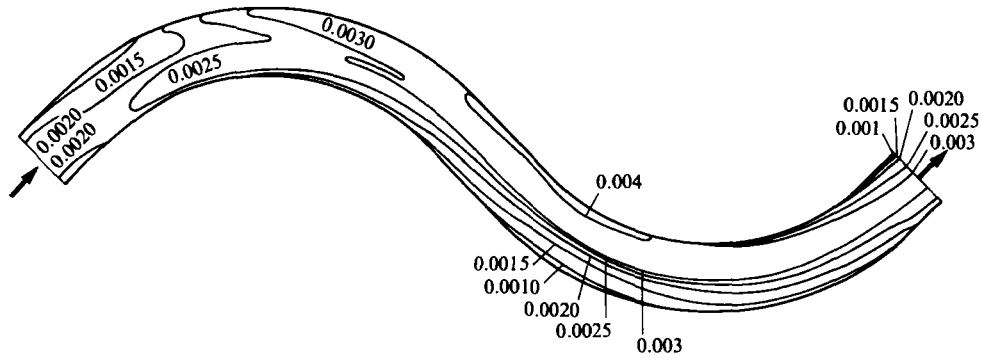

FIGURE 13: Predicted bed-shear-stress distribution $\tau/\rho\bar{U}^2$, case 1.

predictions obtained with the curvature correction agree quite well with the measurements while those without the correction show too little mixing. The same applies to the discharge at the centre (figure 11*b*), though to a lesser extent. On the whole, the rate of mixing as one proceeds downstream from one bend to the other is reproduced quite well. In particular, the model predicts correctly that there is much faster mixing in the case with the central discharge than in the cases with the discharge either at the inner or the outer bank. This is because the diffusivity in the centre of the channel is generally larger than near the banks.

Finally, the predicted and measured depth-averaged concentration profiles for the rough-bed channel are compared in figure 12. Here also, the agreement is generally very good. The profiles show that the pollutant is almost completely mixed across the channel by the second channel wavelength (cross-section 10C). This is in contrast to the corresponding behaviour in case 2 with a smooth bed where at section 10C considerable lateral non-uniformities are still present. The faster mixing in case 3 is due to the much higher diffusivity generated by the rough bed. This behaviour is reproduced very well by the model.

3.3.3. *Bed-shear-stress distribution*

Figure 13 shows the computed bed-shear-stress contours for case 1, i.e. for the flow in the large channel with the high aspect ratio. The bed-shear-stress development can be seen to correspond closely with that of the depth-averaged streamwise velocity. At the entrance to the first bend, the shear-stress distribution is still rather symmetrical. Inside the bend, the maximum shifts first to the inner bank and then to the outer bank towards the exit of the bend, as does that of the streamwise velocity. The development is then reversed in the second bend. The maximum bed shear-stress can be found near the bank connecting the exit part of the outer bank in the first bend with the entrance part of the inner bank of the second bend. The lowest shear stress develops near the outer bank towards the middle of the bend. This result is in agreement with Meckel's (1978) experimental findings that it is the region near the convex wall where bed erosion due to high shear stress takes place and the region near the concave wall where the shear stress is lowest so that sediment is deposited.

4. Conclusions

The review of experiments on curved and meandering open-channel flow presented in this paper has highlighted the complex three-dimensional nature of these flows and established the main mechanisms involved and the interactions between them. In curved open channels, centrifugal forces induce a transverse surface slope and this in turn generates secondary motions when the streamwise velocity is not uniform over the depth, as is the case because of the friction at the bed. The secondary motion is generally towards the inner bank near the bed and towards the outer bank near the surface, but more complex patterns may occur, especially in narrow channels. The strength of this motion may be 40–50 % of the streamwise velocity in tight single bends, but the motion is weaker in meanders owing to the opposite rotation generated in alternate bends. The secondary motion in meanders causes considerable lateral spreading of the pollutants so that the effective mixing is much stronger than in a straight channel. This motion also influences the streamwise velocity distribution over the cross-section, e.g. it causes the observed supression of the velocity maximum below the water surface. Except in cases with very mild curvature, the transverse distribution of this velocity is also influenced markedly by streamwise surface slopes, which are a consequence of the building-up and decay of transverse slopes. The influence of streamwise slopes extends considerably upstream and downstream of the bend so that there is strong interaction between the individual bends in a meandering channel. A review of experiments has shown that developed flow, where the streamwise surface slope is insignificant, occurs very seldom.

On the other hand, the review of theories on meandering-channel flow has shown that most existing methods for calculating this flow are based on the assumption of developed flow. Other methods, which consider the developing nature of the flow, are restricted to relatively mild curvature. The models are therefore not suitable for situations with strong curvature and development regions, where the full three-dimensional nature of the flow has to be accounted for. Also, the existing models for pollutant spreading in meandering channels allow only a fairly crude empirical description of the influence of the curvature via dispersion coefficients and do not describe the actual transport of pollutants by the secondary motion.

A mathematical model has been presented in this paper which takes full account of the complex three-dimensional nature of the flow and pollutant concentration field. The model is an extension of Leschziner & Rodi's (1979) three-dimensional numerical model for single bends to meanders and the solution of the concentration equation. Further, the numerical accuracy has been improved and the standard k–ϵ turbulence model incorporated in the basic model has been modified to account for the effects of streamline curvature on the turbulent transport mechanisms. Applications of the model have been presented for three different meander situations for which velocity and dye concentration measurements in laboratory flumes were available from the literature. The case of a wide, shallow channel (width-to-depth ratio $B/h = 20$) with a smooth bed was considered and two fairly narrow channels ($B/h \approx 5$) with one having a smooth and the other a rough bed. For the wide-flume case, detailed comparisons of the longitudinal and secondary velocity field with the measurements have been carried out. The agreement is generally good; in this case there is basically one large secondary-motion eddy present. For the smooth narrow flume, the predictions yielded a more complex secondary flow pattern with several eddies developing and decaying, but there were no measurements for comparison. For the smooth-bed case, there is again fairly good agreement for the vertical profiles

of longitudinal velocity while the agreement is not so good for the rough-bed case where the behaviour of the experimental profiles is difficult to explain. However, in all cases the development of the depth-averaged longitudinal profile is predicted fairly well, in particular the transverse shift of the velocity maximum as one moves through the bends. The spreading of dye discharge at various locations in the flumes is also predicted quite well in all cases. Only in the narrow-flume situation with a smooth bed was the curvature correction to the turbulence model important because only in this case was the turbulence associated with the horizontal shear layers not overruled by the bed-generated turbulence dominant in shallow-channel and rough-bed situations. The model has been shown to reproduce well the differences between the individual cases, e.g. the influence of discharge location, width-to-depth ratio and roughness. The latter enhances the transverse mixing considerably. It is important to note that all the results were obtained without any tuning of the empirical constants. As the spreading of dye in meandering channels is dominated by the secondary motion, the correct simulation of this spreading is also an indirect demonstration that the secondary motion has been predicted realistically. Finally, the bed shear stress, which is responsible for erosion of beds, has been found to follow closely the depth-averaged velocity distribution.

Although the results obtained with the model described in this paper are generally satisfactory, further testing should be carried out. This is unfortunately made difficult by the lack of suitable experimental data. In particular, the development of the secondary motion in narrow channels, the influence of roughness and the distribution of the bed shear stress should be studied further in some detail. In future, the model should also be extended to, and tested for, non-rectangular-channel situations occurring in real life. Finally, it should be pointed out that the results of the three-dimensional model can be and have been used to determine the lateral dispersion coefficients required in simpler, two-dimensional depth-averaged models (see Pavlovic & Rodi 1985).

The work reported here was sponsored by the Deutsche Forschungsgemeinschaft via the Sondersforschungsbereich 80. The calculations were carried out on the Siemens 7880 computer of the University of Karlsruhe, using a highly modified version of the program FLAIR of CHAM Ltd., London, which is based on the algorithms of Patankar & Spalding (1972) and Pratap & Spalding (1976).

REFERENCES

ANANYAN, A. K. 1957 Dvizhenie zhidkosti na povorote vodovoda. Erevan: *Izd. Akad. Nauk. Arm. SSR.* [Transl. 1965 *Fluid Flow in Bends of Conduits.* Jerusalem: Israel Program Sci. Transl.]

BOUSSINESQ, J. 1868 Mémoire sur l'influence des frottements dans les mouvements reguliers des fluides. *J. Math. Pures Appl.* (2me sér.) **13**, 377–424.

BRADSHAW, P. 1973 Effects of streamline curvature on turbulent flow. *AGARDograph* 169.

CALLANDER, R. A. 1969 Instability and river channels. *J. Fluid Mech.* **36**, 465–480.

CALLANDER, R. A. 1978 River meandering. *Ann. Rev. Fluid Mech.* **10**, 129–158.

CHANG, Y. C. 1971 Lateral mixing in meandering channels, Ph.D. thesis, University of Iowa, USA.

DEMUREN, A. O. 1983 Three-dimensional numerical computation of flow and pollutant dispersion in meandering channels. In *Proc. 20th Congress of the IAHR, Moscow, USSR*, Vol. III, pp. 29–36.

DE VRIEND, H. J. 1973 Theory of viscous flow in wide curved open channels. In *Proc. IAHR Intl. Symp. on River Mechanics, Bangkok, Thailand.*

DE VRIEND, H. J. 1979 Flow measurements in a curved rectangular channel. *Delft University of Technology, Dept. of Civil Engng, Laboratory of Fluid Mechanics, Internal Rep.* 9–79.

DE VRIEND, H. J. 1981*a* Velocity redistribution in curved rectangular channels. *J. Fluid Mech.* **107**, 423–439.

DE VRIEND, H. J. 1981*b* Steady flow in shallow channel bends. *Comm. on Hydraulics, Delft University of Technology, Rep. No.* 81–3.

DE VRIEND, H. J. 1981*c* Steady flow in shallow channel bends. Doctoral dissertation, Delft University of Technology.

EINSTEIN, H. A. & HARDER, J. A. 1954 Velocity distribution and boundary layer at channel bends. *Trans. Am. Geophys. Union* **35**, 114–120.

ELDER, J. W. 1959 The dispersion of marked fluid in turbulent shear flow. *J. Fluid Mech.* **5**, 544–560.

ENGELUND, F. 1974 Flow and bed topography in channel bends. *J. Hydraul. Div. ASCE* **100** (HY11), 1631–1648.

FISCHER, H. B. 1969 The effects of bends on dispersion in streams. *Wat. Resources Res.* **5**, 496–506.

FISCHER, H. B., LIST, E. J., KOH, R. C. Y., IMBERGER, J. & BROOKS, N. H. 1979 *Mixing in Inland and Coastal Waters.* Academic.

FUKUOKA, S. 1971 Longitudinal dispersion in sinous channels. Ph.D. thesis, University of Iowa, USA.

FUKUOKA, S. & SAYRE, W. W. 1973 Longitudinal dispersion in sinous channels. *J. Hydraul. Div. ASCE* **99** (HY1), 195–217.

GIBSON, M. M. 1978 An algebraic stress and heat-flux model for turbulent shear flow with streamline curvature. *Intl. J. Heat Mass Transfer* **21**, 1609–1617.

GIBSON, M. M. & RODI, W. 1981 A Reynolds stress closure model of turbulence applied to the calculation of a highly-curved mixing layer. *J. Fluid Mech.* **103**, 161–182.

HOLLEY, E. R. & ABRAHAM, G. 1973 Field tests on transverse mixing in rivers. *J. Hydraul. Div. ASCE* **99** (HY12), 2313–2331.

IKEDA, S. 1975 On secondary flow and bed profile in alluvial curved open channels. In *Proc. 16th Congress of the IAHR, Sao Paulo, Brazil*, Vol. 2, pp. 105–112.

IPPEN, A. T., DRINKER, P. A., JOBIN, W. R. & SHEMDIN, O. H. 1962 Stream dynamics and boundary shear distributions for curved trapezoidal channels. *MIT Hydrodynamics Lab. Rep. No.* 47.

LAUNDER, B. E., REECE, G. J. & RODI, W. 1975 Progress in the development of a Reynolds stress turbulence closure, *J. Fluid Mech.* **86**, 737–566.

LAUNDER, B. E. & SPALDING, D. B. 1974 The numerical computation of turbulent flow. *Comp. Meth. Appl. Mech. & Engng* **3**, 269–289.

LEONARD, B. P. 1979 A stable and accurate convective modelling procedure based on quadratic upstream interpolation. *Comp. Meth. Appl. Mech. & Engng* **19**, 59–98.

LEOPOLD, L. B. & WOLMAN, M. G. 1957 River channel patterns: braided, meandering and straight. *US Geol. Surv. Prof. Paper* 282-B, pp. 37–86.

LESCHZINER, M. A. & RODI, W. 1979 Calculation of strongly curved open channel flow. *J. Hydraul. Div. ASCE* **105** (HY10), 1297–1314.

LESCHZINER, M. A. & RODI, W. 1981 Calculation of annular and twin parallel jets using various discretisation schemes and turbulence-model variations. *Trans. ASME: J. Fluids Engng* **103**, 352–360.

MCGUIRK, J. & RODI, W. 1977 A mathematical model for a vertical jet discharging into a shallow lake. In *Proc. 17th Congress of the IAHR, Baden Baden, F.R. Germany.*

MECKEL, H. 1978 Spiralströmung und Sedimentbewegung in Fluß- und Kanalkrümmungen. *Wasserwirtschaft* **68**, 287–294.

MECKEL, H. & CHUN, V. H. 1975 Einfluß der Sohlausbildung auf die Strömungsverhältnisse, in Gerinnebögen. In *Leitmotiv Wasser* (ed. W. Buck & H. H. Bernhart). Universität Karlsruhe.

MOCKMORE, C. A. 1943 Flow around bends in stable channels. *Trans. ASCE* **109**, 593–619.

MOSONYI, E. & GÖTZ, W. 1973 Secondary currents in subsequent model bends. In *Proc. Intl. Symp. on River Mechanics, IAHR, Bangkok, Thailand.*

MOSONYI, E., MECKEL, H. & MEDER, G. 1975 Etude de développement du courant spiral dans de courbes consecutives d'un canal. In *Proc. 16th congress of the IAHR, São Paulo, Brazil*, Vol. 2, pp. 347–355.

PATANKAR, S. V. & SPALDING, D. B. 1972 A calculation procedure for heat, mass and momentum transfer in 3D parabolic flows. *Intl. J. Heat Mass Transfer* **15**, 1878–1806.

PAVLOVIC, R. N. & RODI, W. 1985 Depth-averaged numerical predictions of velocity and concentration fields in meandering channels. In *Proc. 21st Congress of the IAHR, Melbourne, Australia*, pp. 121–125.

PRATAP, V. S. & SPALDING, D. B. 1976 Fluid flow and heat transfer in three-dimensional duct flows. *Intl. J. Heat Mass Transfer* **19**, 1183–1188.

RASTOGI, A. K. & RODI, W. 1978 Predictions of heat and mass transfer in open channels, *J. Hydraul. Div. ASCE* (HY3), 397–420.

RODI, W. 1980 *Turbulence Models and Their Applications in Hydraulics*. Delft: International Association for Hydraulic Research.

RODI, W., PAVLOVIC, R. & SRIVATSA, S. K. 1981 Prediction of flow and pollutant spreading in rivers. In *Transport Models for Inland and Coastal Waters* (ed. H. B. Fischer), pp. 63–111. Academic.

RODI, W. & SCHEUERER, G. 1983 Calculation of curved shear layers with two-equation turbulence models, *Phys. Fluids* **26**, 1422–1436.

ROZOVSKII, I. L. 1957 Dvizhenie vody na povorote otkrytogo rusla. Kiev: *Izd. Akad. Nauk. Ukr. SSR*. [Transl. 1961, *Flow of Water in Bends of Open Channels*. Jerusalem, Israel Program Sci. Transl.]

SHURKY, A. 1949 Flow around bends in an open flume. *Trans. ACSE* **115**, 751–779.

SIEBERT, W. 1980 Strömungscharakteristiken in einem Kanal mit 180°-Krümmungen, Ph.D. thesis, University of Karlsruhe.

SIEBERT, W. & GÖTZ, W. 1975 A study on the deformation of secondary flow in models of rectangular meandering channels. In *Proc. 16th Congress of the IAHR, São Paulo, Brazil*, Vol. 2, pp. 142–149.

SMITH, R. 1981 Effects of non-uniform currents and depth variations upon steady discharges in shallow water. *J. Fluid Mech.* **110**, 373–380.

SMITH, R. 1982 Where to put a steady discharge in a river. *J. Fluid Mech.* **115**, 1–11.

SMITH, R. 1983 Longitudinal dispersion coefficients for varying channels. *J. Fluid Mech.* **130**, 299–314.

TAMAI, N., IKEUCHI, K., YAMAZAKI, A. & MOHAMED, A. A. 1983 Experimental analysis on the open channel flow in rectangular continuous bends. *J. Hydrosci. & Hydraul. Engng* **1**, 17–31.

TAYLOR, G. I. 1954 The dispersion of matter in turbulent flow through a pipe. *Proc. R. Soc. Lond.* A**219**, 186–203.

THOMSON, J. 1876 On the origin of windings of rivers in alluvial plains with remarks on the flow of water round bends in pipes. *Proc. R. Soc. Lond.* **25**, 5–8.

YEN, B. C. 1965 Characteristics of subcritical flow in a meandering channel. *Inst. of Hydr. Res., University of Iowa, Rep.*

YEN, C. L. 1970 Bed topography effect on flow in a meander. *J. Hydraul. Div. ASCE* **96** (HY1), 57–73.

YOTSUKURA, N., FISCHER, H. B. & SAYRE, W. W. 1970 Measurements of mixing characteristics of the Missouri River between Sioux City, Iowa and Plattsmouth, Nebraska. *US Geological Survey Water-Supply Paper* 1899-G.

YOTSUKURA, N. & SAYRE, W. W. 1976 Transverse mixing in natural channels. *Wat. Resources Res.* **12**, 695–704.